行政院國家科學委員會專題研究計畫　期中進度報告

封裝系統(SOP)內部微縮化被動元件的分析與設計(2/3)

計畫類別：個別型計畫
計畫編號：NSC93-2213-E-002-034-
執行期間：93 年 08 月 01 日至 94 年 07 月 31 日
執行單位：國立臺灣大學電信工程學研究所

計畫主持人：江簡富

報告類型：精簡報告
報告附件：出席國際會議研究心得報告及發表論文
處理方式：本計畫可公開查詢

中　華　民　國 95 年 2 月 27 日

封裝系統(SOP)內部微縮化被動元件的分析與設計（2/3）

NSC 93-2213-E-002-034

PI: Jean-Fu Kiang

Department of Electrical Engineering and
Graduate Institute of Communication Engineering
National Taiwan University
No.1, Sec. 4, Roosevelt Road, Taipei, Taiwan, ROC

The contents of this annual report consist of four parts. The first part, "design of dedicated short-range communication transceiver" summarizes the design of an RF transceiver, the second part, "3-bit vector-sum phase shifter using switched attenuator" summarizes the design of a phase shifter in steps of 45 degrees, the third part, "size-reduction of patch and meshed antenna using inductors" presents a miniaturized meshed antenna, the fourth part, "analysis of range detection system" presents a small range-detection system. All these four parts are designed at 2.5 GHz, and will be integrated in the next phase for demonstration.

Design of Dedicated Short-Range Communication (DSRC) Transceiver

Abstract — In this part, a short-range communication system is designed in the 2.43 GHz ISM band. It includes LNA, mixer, and LO. The LO signal is stablized by an injection-locking oscillator. IF amplifiers and filters are designed to improve the IF signal quality. This hybrid circuit is implemented on FR4 PCB to verify its function.

Key Words —LNA, mixer, injection-locking oscillator, short-range communication system.

I. INTRODUCTION

In this work, a dedicated short-range communication (DSRC) system is designed for vehicular communication, in which modulated codes are transmitted over the air to inform other vehicles of relevant traffic situation. Fig.1 shows the architecture of the transceiver.

In the transmitter, the modulated instruction is processed by the IF circuit and up-converted to an RF signal by an up-conversion mixer, amplified and sent to the antenna for transmission. In the receiver, the signal received by the antenna is amplified by a low-noise amplifier, then down-converted to an IF signal by a down-conversion mixer. The IF signal is demodulated and decoded to retrieve the instruction. The RF and LO signals are at 2.431 GHz and 2.43 GHz, respectively, rendering 1 MHz signal at the IF port.

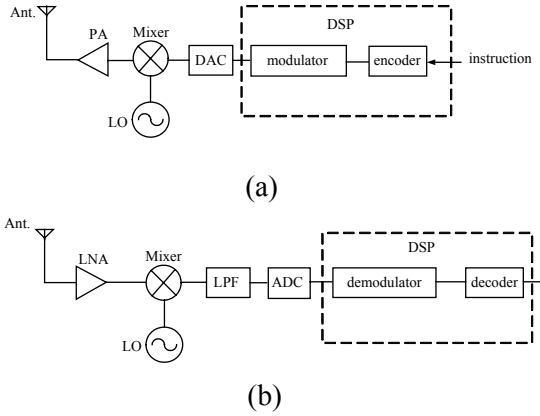

Figure 1 : architecture of DSRC (a) transmitter and (b) receiver.

In a direct-conversion receiver, all the in-band channels are down-converted directly to the baseband using a single mixer [2]

A conventional RF circuit usually consists of low-noise amplifier (LNA), local oscillator, mixer and filter. The LNA amplifies the desired RF signal with very low additional noise. The mixer mixes the amplified RF signal with the LO signal to render an IF signal. Filters are used to suppress undesired harmonics and noise. Signal from the local oscillator may leak to the antenna because its frequency is close to that of the RF signal. The leaky LO signal may be routed to the receiver, mixing with the local oscillator to result in a time-varying dc offset at the IF output.

II. COMPONENTS OF SYSTEM

A. LNA

Fig. 2 shows the low-noise amplifier circuit diagram. In microwave circuits, power gain is more frequently specified than voltage gain [3]. The source impedance and load impedance should be conjugate matched to achieve maximum power gain.

The noise figure F quantifies the performance of a noisy microwave amplifier, which is defined as the ratio of the total available noise power at the output of the

amplifier to the available noise power at the output due to the thermal noise from the input termination alone.

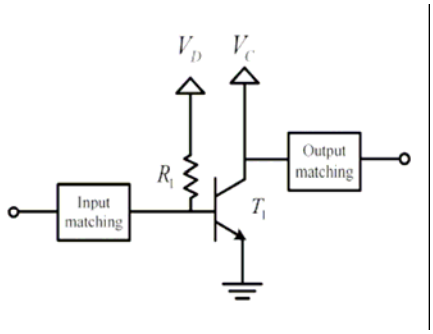

Figure 2 : LNA circuit.

Nonlinearity can be revealed as variation of the small-signal gain with the input level. Such effect can be quantified by the 1-dB compression point, defined as the input signal level at which the small-signal gain drops by 1 dB.

If a weak signal is input to the nonlinear system accompanied by two strong interferers, one of the IM products may fall in the band of interest and corrupt the desired signal. Fig.3 shows the definition of the third-order intercept point (IP3). The IP3 can be measured by a two-tone test when A is sufficiently small so that the gain α_1 is relatively constant and the higher-order nonlinear terms are negligible. When A is increased, the fundamentals increase in proportion to A, whereas the third-order IM products increase in proportion to A_3. The IP3 can be determined as the intersection of these two lines. The abscissa and the ordinate of this point are called the input IP3 (IIP3) and the output IP3 (OIP3), respectively.

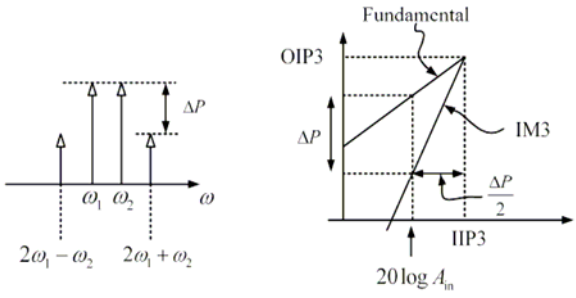

Figure 3 : Determination of IP3.

B. Diode Mixer

A mixer also contributes noise and degrades the signal-to-noise ratio of the signals. Conversion gain from RF to IF can be positive or negative, and a negative conversion gain is also called a conversion loss. The RF and LO ports are typically matched to 50Ω while the impedance of the IF port is matched to that of the IF filter. Impedance matching at the RF and IF ports is necessary to avoid signal reflection and excessive passband ripple in the filters [4].

Typically, return loss of less than 10 dB is required. On the other hand, specification of return loss at the LO port is less strict. However, excessive return loss demands the LO to deliver more power and may cause LO-pulling problem. The isolation between LO and RF ports is critical as the LO-to-RF feedthrough may result in LO signal leaking to the antenna and corrupting the desired RF signals.

Fig.4 shows an example of balanced mixer which consists of two identical single-ended mixers connected to a 3-dB coupler.

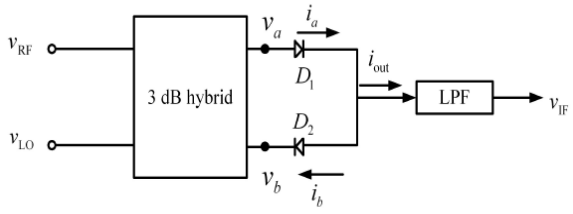

Figure 4 : Schematic of balanced mixer.

With perfectly matched diodes and perfect 3-dB coupler, no LO signal will leak to the IF and RF ports, and the attenuation between the RF and the IF ports is insignificant [7].

C. Local Oscillator

A microwave oscillator is a one-port device to generate stable sinusoidal signal based on a self-sustaining mechanism. An oscillator can also be viewed as two one-port networks connected back to back. Noise is injected into an oscillator by internal or external devices, and may affect both the frequency and amplitude of the output signal [2].

The phase noise of an LC tank is determined by its Q factor. A higher Q factor implies sharper skirt around the resonant frequency. The Q factor is an indicator of how much energy is lost as it is transferred between the electric form and the magnetic form. Fig.5 shows the local oscillator circuit diagram.

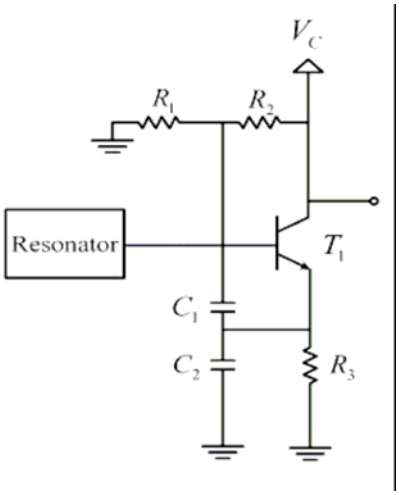

Figure 5 : Local oscillator.

In order to stabilize the local oscillator frequency, injection-locking oscillator is designed to lock the frequency. Fig.6 shows the circuit diagram of an injection-locking oscillator. At small injection level, the locking range is related to the injection signal power by (1) where P_{inj} is the injection power, P_0 is the output power of the free-running oscillator, f_{free} is the free-running frequency, Q_{ext} is the external Q factor of the resonant circuit [9].

$$\Delta f = \frac{2 f_{free}}{Q_{ext}} \sqrt{\frac{P_{inj}}{P_0}} \qquad (1)$$

Adjusting the injection power only affects the ILO locking range, but not the free-running frequency of the oscillator [6].

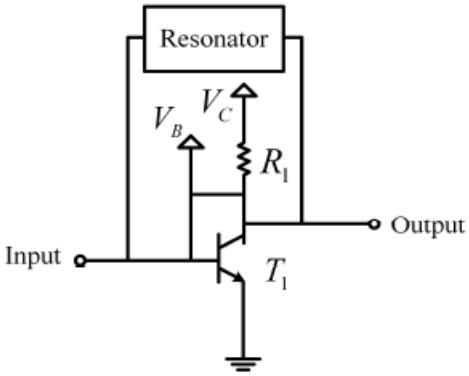

Figure 6 : Injection-locking oscillator.

III. RESULTS

The simulated and measured S parameters of LNA are shown in Fig.7. The power gain is about 16 dB and the return loss is about -30 dB. The simulated IIP3 and OIP3 are 6.09 dB and 21.72 dB, respectively, the measured IIP3 and OIP3 are 4.59 dB and 20.26 dB, respectively.

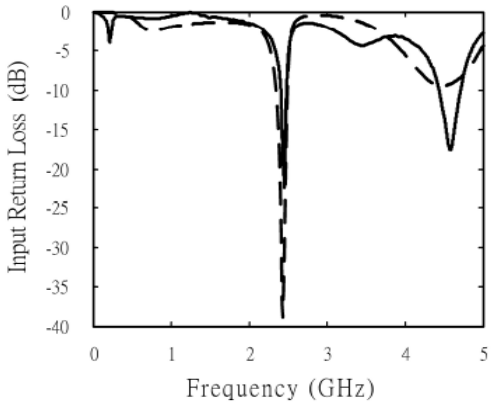

(a)

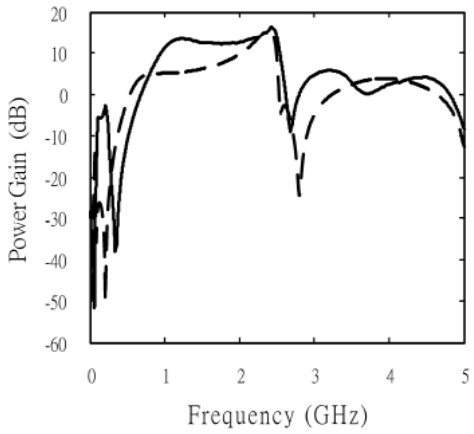

(b)

Figure 7 : S parameter of LNA, (a) input return loss, (b) power gain, -- : simulated, - : measurement.

Simulation results of conversion loss and the return loss are shown in Fig.8. At 2.43 GHz, the conversion loss is 7.4 dB and the return loss is 21.7 dB. The measured conversion loss is 10 dB and the measured RF return loss is 12 dB. The isolation between RF and LO is 15 dB.

Fig.9 shows the measured ILO signal. Its output power is 8.5 dBm and its phase noise is -101 dBc/Hz at 100 kHz offset

Finally, LNA, mixer and ILO are integrated into a single circuit board as shown in Fig.10. A 2.431 GHz RF signal is mixed with the LO signal to generate an IF signal.

IF amplifier and bandpass filter are designed to get the desired frequency at 1 MHz. The measured spectrum is shown in Fig.11.

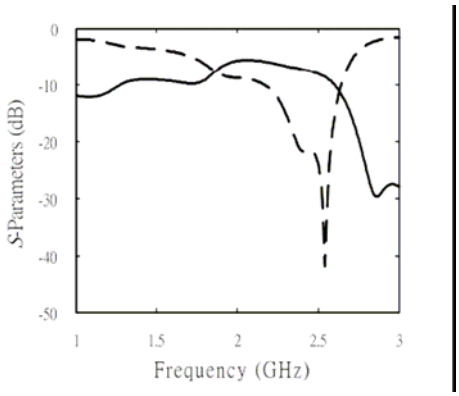

Figure 8 : Simulated conversion loss and return loss of diode mixer, --: S11, -: S21.

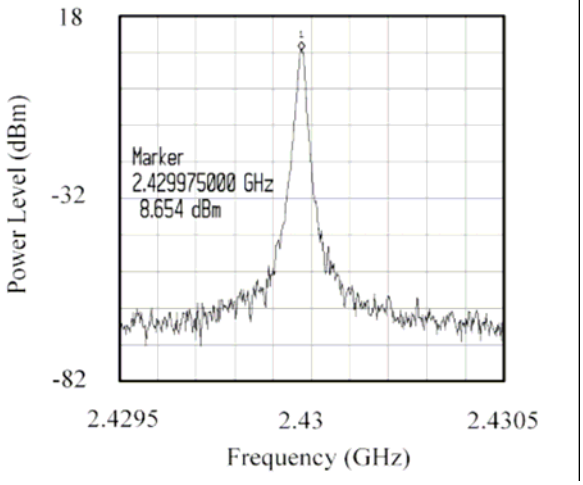

Figure 9 : Measured spectrum of ILO with PLL injection.

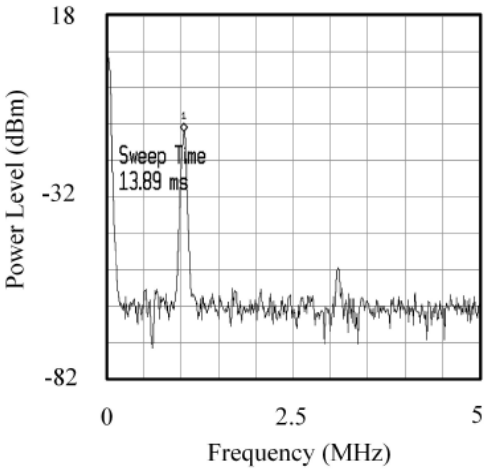

Figure10 : Measured IF spectrum centered at 1 MHz.

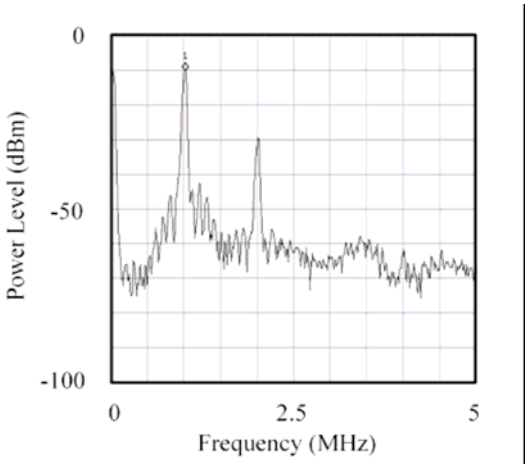

Figure11 : Measured IF spectrum after IF amplifier and bandpass filter.

VI. Conclusion

In this part, key components of a typical RF front-end have been designed and integrated to build a prototype of dedicated short-range communication (DSRC) transceiver. IF amplifier and filter are also designed to improve the IF signal. The RF front-end is designed in the ISM band at 2.431GHz and generate 1 MHz IF signal. Injection-locking oscillator and good resonator are used to stabilize the LO signal with PLL and crystal oscillator, respectively, as reference signal source.

REFERENCES

[1] G. Gonzalez, *Microwave Transistor Amplifiers Analysis and Design*, Prentice Hall, 1997..
[2] B. Razavi, *RF Microelectronics*, Prentice Hall, 1998.
[3] U. L. Rohde and D. P. Newkirk, *RF/Microwave Circuit Design for Wireless Applications*, Wiley, 2000.
[4] F. Giannini and G.Leuzzi, *Nonlinear Microwave Circuit Design*, Wiley, 2004.
[5] B. Razavi, *Design of Analog CMOS Integrated Circuits*, McGraw-Hill, 2001.
[6] C. C. Huang and T. H. Chu, ``Analysis of MESFET injection-locked oscillators in fundamental mode of operation," *IEEE Trans. Microwave Theory Tech.*, vol.42, pp.1851-1857, Oct. 1994.
[7] S. Long, ``Fundamentals of mixer design," *Agilent Design Seminar*, Apr. 2001.

A 3-Bit Vector-Sum Phase Shifter Using Switched Attenuator

Abstract — A new 3-bit vector-sum phase shifter using switch attenuator is proposed in this part. Four switched attenuators replace the four amplifiers in the previous work and thus constitute a passive phase shifter. This phase shifter consumes no dc power, has simpler structure and broader bandwidth than previous work, and is suitable for microwave technology.

Index terms — phase shifter, vector sum, attenuator, digital, switch.

I. INTRODUCTION

The phase shifter plays an important role in phased-array antenna and smart antenna systems with beam-forming capability. The digital phase shifter is less dependent on component variations and can be easily controlled by digital control signals.

An active vector-sum phase shifter in the frequency range of 2.2~2.3 GHz was proposed in [1]. The circuit diagram is shown in Fig. 1. However, the variance between each variable-gain amplifier (VGA) is hard to be reduced and somehow degrades the accuracy of the phase shifter.

In this part, a 3-bit vector-sum phase shifter is proposed. With similar theory and architecture to that in [1], this phase shifter replaces the four VGAs by four switched attenuators in Fig. 1. The switched attenuator has insertion loss of 0 dB or 7.66 dB, depending on the control states, the loss difference of the switched attenuator is the same as the gain difference of the VGA used in [1]. The switched attenuator at two different loss states inherently provide nearly the same phase shift at the desired frequency. Since there is no power consumption in these attenuators, the power consumption of this phase shifter is approximately zero. It is much easier for the switched attenuator to perform broadband input/output matching without additional matching circuit which may be needed in VGAs, and thus the circuit size can be further reduced.

We will first describe the vector-sum method which is adopted in this work. A 3-Bit vector-sum phase shifter using switched attenuator designed at 2.45 GHz is then presented with the simulation results.

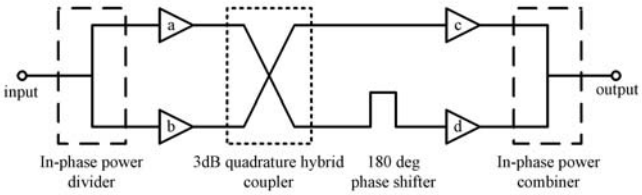

Figure 1 : Schematic diagram of the vector-sum phase shifter proposed in [1].

II. BACKGROUND

Fig. 1 shows the scheme of a vector-sum phase shifter. The input signal is first evenly divided into two ways and the two signals are multiplied by *a* and *b* which are the complex gain/attenuation factors. The multiplied signals are then passed through a 3-dB branch-line coupler and linearly combined at the two output ports. One of these two signals will be delayed by 180° and then multiplied by *d*. The other is directly multiplied by *c* where *c* and *d* are also complex gain/attenuation factors. When the VGAs are used in this circuit, the magnitude of the gain/attenuation factors are greater than unity. However, if the switched attenuators are adopted, the factors will be less than unity. The transfer function of this phase shifter, T , can be derived as

$$T = (bc - ad)/2 + j(ac - bd)/2 \qquad (1)$$

where $j = \sqrt{-1}$.

Assume that *a*, *b*, *c*, and *d* are all positive real number without loss of generality, the transfer function can then be thought of as a sum of four vectors of magnitude *bc*, *ad*, *ac*, *bd* lying on the axes and pointing outward from the origin as shown in Fig.2 . Since *a*, *b*, *c*, and *d* can be arbitrarily selected, the four vectors can be independently adjusted, and the transfer function can be generated with arbitrary phase angle.

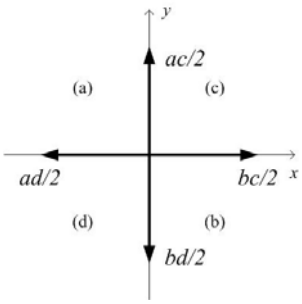

Figure 2 : Vector decomposition diagram of the transfer function.

A. Analog Control Method

It is realized that any output signal of this phase shifter is available with suitable VGAs or switched attenuators. However, some other constraints are improved in real application.

It is always better to limit the output signal of various phases to the same signal level. The gain or attenuation change of continuous phase variance is preferred to be continuous. Moreover, for power efficiency, only two adjacent vectors are needed to form an output signal in any one quadrant in Fig. 2, namely, only three out of *a*, *b*, *c*, *d* are necessary.

A set of gain/attenuation factors have been derived under such constraints assuming that all the gain/ attenuation factors have zero phase shift. The gain/ attenuation factors versus phase shift range are listed in Table I, where M is a positive real number and θ is the desired phase shift. If the gain/attenuation factors contain additional phase shift of the same value, the output signal will be phase-shifted by a constant value.

TABLE I
GAIN VARIANCE OF THE VARIOUS PHASES OF THE OUTPUT SIGNAL

	0°~90°	**90°~180°**	**180°~270°**	**270°~360°**
a	Msinθ	M	-Mcosθ	0
b	Mcosθ	0	-Msinθ	M
c	M	Msinθ	0	Mcosθ
d	0	-Mcosθ	M	-Msinθ

B. Digital Control Method

For applications which requires no continuous phase variance or for convenience of digital control, the following digital method has been developed in [1]. The VGAs or switched attenuators have to attend two states : high- and low-gain states (low- and high-attenuation states) to realize a 3-bit phase shifter. Table II shows all the combination of different control states and their corresponding output results. To obtain output signals of constant level, one of the following two equations must be satisfied.

$$M^2(1-k)/\sqrt{2} = M^2\left(1-k^2\right)/2 \qquad (2)$$

$$kM^2(1-k)/\sqrt{2} = M^2\left(1-k^2\right)/2 \qquad (3)$$

where M and k are both positive real numbers, and k is less than unity. There is only one solution from (2), $k=\sqrt{2}-1$, which implies that the two states of the VGAs or attenuators must have 7.66 dB ($-20\log(\sqrt{2}-1)$) gain/ attenuation difference. The control states with phase shift is listed in Table III, where H represents the high-gain or low-attenuation state while L represents the low-gain or high- attenuation state.

C. Switched Attenuators

In this part, four switched attenuators shown in Fig. 3 are used to replace the four VGAs in [1]. The switched attenuator is ideally composed of two single-pole double-throw (SPDT) switches and a T-section resistor attenuator. The value of R1 and R2 can be determined as

$$\mathrm{R1} = Z_0\frac{1-k}{1+k} \qquad (4)$$

$$\mathrm{R2} = Z_0\frac{2k}{1-k^2} \qquad (5)$$

$$\mathrm{R1} = Z_0\frac{1-k}{1+k} \qquad (4)$$

$$\mathrm{R2} = Z_0\frac{2k}{1-k^2} \qquad (5)$$

TABLE II
OUTPUT SIGNALS OF VARIOUS CONTROL STATES

		a=M b=M	a=kM b=kM	a=kM b=M	a=M b=kM
c=M d=M	Phase			**315°**	**135°**
	Magnitude	0	0	$(1-k)M^2/\sqrt{2}$	$(1-k)M^2/\sqrt{2}$
c=kM d=kM	Phase			315°	135°
	Magnitude	0	0	$k(1-k)M^2/\sqrt{2}$	$k(1-k)M^2/\sqrt{2}$
c=kM d=M	Phase	**225°**	225°	**270°**	**180°**
	Magnitude	$(1-k)M^2/\sqrt{2}$	$k(1-k)M^2/\sqrt{2}$	$(1-k^2)M^2/2$	$(1-k^2)M^2/2$
c=M d=kM	Phase	**45°**	45°	**0°**	**90°**
	Magnitude	$(1-k)M^2/\sqrt{2}$	$k(1-k)M^2/\sqrt{2}$	$(1-k^2)M^2/2$	$(1-k^2)M^2/2$

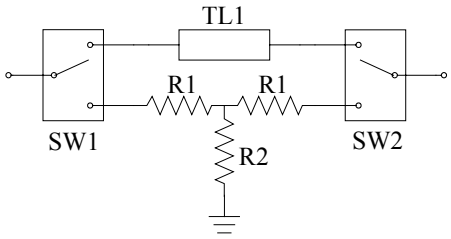

Figure 3 : Scheme of the switched attenuator.

where Z_o is the characteristic impedance of the transmission line. Substituting $k=\sqrt{2}-1$ and $Z_0=50\Omega$ into (4) and (5), R1 and R2 are found to be $20.7\,\Omega$ and $52.5\,\Omega$, respectively.

The transmission line TL1 is unavoidable in practice, and may cause phase difference between the two states of the switched attenuator. This will results in phase and magnitude deviation of the overall system.

III. SIMULATION **R**ESULTS

A 3-bit vector-sum phase shifter has been designed at 2.45 GHz and simulated using Advanced Design System (ADS). Fig. 4 shows the insertion loss S21 of the phase shifter under various attenuation states. Each black point in Fig. 4 has a corresponding entry in Table II, and only

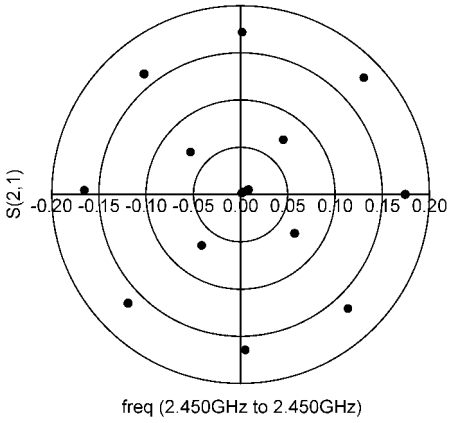

Figure 4 : Simulated S21 of all combination of attenuation states.

the outer eight points contribute to the 3-bit phase shifting. The outer eight points are almost in the same attenuation level of about -15.5 dB with the mean value and the standard deviation of the phase difference between adjacent two points of 45.0° and 3.2°, respectively.

Fig. 5 shows the phase shift of the phase shifter over 2.4~2.5 GHz range. The attenuation level of the eight states are limited between -14 and –16 dB, and the phase shift curves are almost parallel to each other, which implies that the proposed phase shifter works from 2.4 to 2.5 GHz.

Since most practical factors have been taken into consideration, the simulation results are expected to be close to the measurement results.

VII. Conclusion

A novel 3-bit vector-sum phase shifter using switched attenuator has been proposed and demonstrated. The switched attenuator is employed to provide the desired attenuation difference of 7.66 dB. The use of switched attenuator eliminates the dc power consumption and reduces the circuit area. The T-section resistor attenuator exhibits a constant insertion loss and almost zero phase shift over a very wide frequency range. The simulation results show that the average phase shift between two adjacent states is 45.0°, and the average attenuation is -15.5 dB.

TABLE III
CONTROL STATES FOR THE EIGHT PHASES OF THE OUTPUT SIGNAL

	0°	**45°**	**90°**	**135°**	**180°**	**225°**	**270°**	**315°**
a	L	H	H	H	H	H	L	L
b	H	H	L	L	L	H	H	H
c	H	H	H	H	L	L	L	H
d	L	L	L	H	H	H	H	H

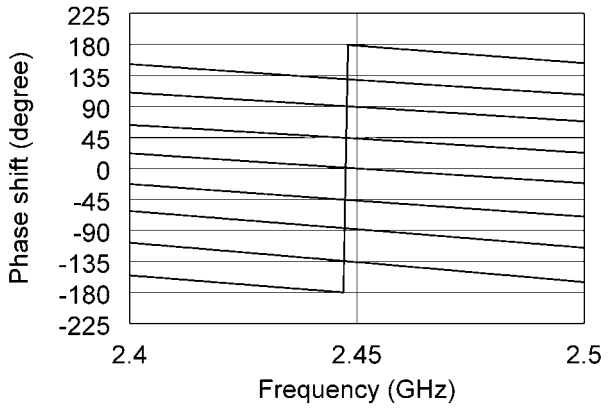

Figure 5 : Shifted angle of the phase shifter under different states

REFERENCES

[1] S. J. Kim and N. H. Myung, "A new active phase shifter using a vector sum method," *IEEE Microwave Guided Wave Lett.*, vol. 10, pp. 233–235, June 2000.

[2] D. M. Pozar, *Microwave Engineering*. New York: Wiley, 1998, pp.364–368.

[3] P. Y. Chen, T.W. Huang, H. Wang, Y.C. Wang, C.H. Chen, and P.C. Chao, "K-band HBT and HEMT monolithic active phase shifters using vector sum method," *IEEE Trans. Microwave Theory Tech.*, vol. 52, pp. 1414-1424, May 2004.

[4] G. Gonzalez, *Microwave Transistor Amplifiers Analysis and Design*. Prentice Hall, 1996.

Size-Reduction of Patch and Meshed Antenna Using Inductors

Abstract — In this part, a patch antenna embedding circular spiral inductors is proposed. These inductors introduce additional phase to the current path and extend its equivalent electrical length. Measurement results indicate that the resonant frequencies of inductor-embedded antennas can be significantly reduced. The effect of different spiral inductor parameters on the resonant frequency is also studied. Measured radiation patterns are close to those of conventional microstrip antennas.

Key Words —Microstrip antenna, spiral inductors.

I. INTRODUCTION

Lumped inductors and capacitors can be cascaded to incur phase delay like a transmission line. Due to this effect, inductors and capacitors implemented in various types have been used to reduce the size of passive components such as antennas [1]-[10].

Dipole antennas have been widely used in radio, television, and cellular phone. The current distribution along a dipole is a standing-wave, and its resonant frequency is determined by the electrical length of the dipole. It is observed that a monopole with a series lumped inductor near its feeding point has a lower resonant frequency because the inductor introduces additional phase delay along the current path [1]. The resonant frequency of a printed dipole can also be reduced by using series inductors implemented by meandering a strip [2].

A resonant slot antenna can be modeled as a half-wavelength transmission line short circuited at both ends. The guided wavelength of the resonant slot-line can be reduced by cutting thin slits along the slot-line to increase its per-unit-length inductance [3], [4]. Loading a short-circuited spiral inductor at the end of the slot antenna has also been proposed [5]-[7].

Spiral antennas are known to have broad bandwidth in input impedance, gain and circular polarization. The operating frequency of spiral antenna can be reduced by loading reactive elements to increase its per-unit-length inductance or capacitance, hence slow down the guided wave along the spiral antennas [8].

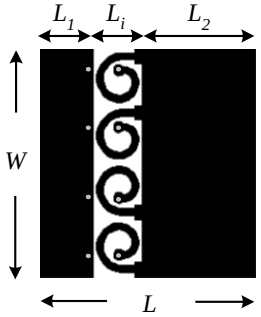

Figure 1 : Patch antenna embedding spirals.

In [9], two patch antennas are connected by thin metal strips or lumped inductors which act as delay lines or phase shifter to the current path, hence reducing its resonant frequency. Inductors have also been inserted in an inverted-F antenna to reduce its resonant frequency [10].

In summary, inductors connected in series with the antennas can be used to reduce their operating frequencies. In this part, inductors will be implemented on patch antennas to reduce their resonant frequencies. The effects of geometrical parameters of spiral inductor on the resonant frequency will also be studied.

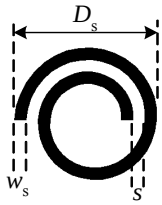

Figure 2 : Enlarged spiral inductor.

II. Patch antenna embedding spiral inductors

A lumped inductor does not behave as an inductor at a relatively high frequency due to its self-resonance and parasitics. Hence, spiral inductors are proposed to substitute for the lumped inductors. Fig.1 shows a patch antenna embedding four spiral inductors that are enlarged in Fig.2. Vias with diameter of 1 mm are used to connect inductors to patches, which contribute parasitic inductance. A metal strip is printed under the upper substrate to connect both vias.

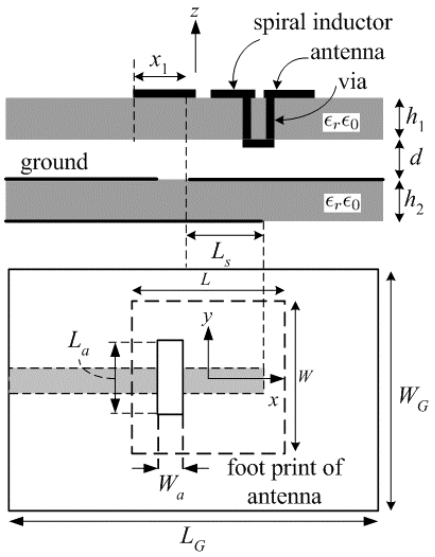

Figure 3 :Aperture-coupling feeding structure.

The circular spiral inductor has strip width w_s, turn spacing s, and outer diameter D_s. The two patches have dimension of $W \times L_1$ and $W \times L_2$, respectively, and is separated by L_i. The spiral inductors can be of square or circular shape. A circular shape exhibits less metal resistance with a given value of inductance and strip

width. In a spiral inductor, the internal turns contribute little inductance while contributing most of the loss [11]. Thus, removal of the first one or two inner turns will slightly increase the *Q*-factor.

Fig. 3 shows the feeding structure of the patch antenna embedding spiral inductors. The aperture-coupling mechanism is more flexible to achieve good input impedance. The patch and the microstrip line are separted by a ground planeto aviod interference and suppress undesired radiation from the feeding structure. The input impedance can be tuned by adjusting the aperture size.

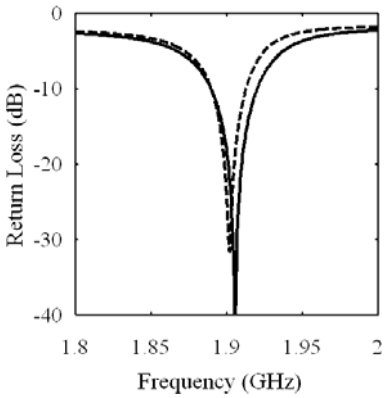

Figure 4 : Radiation pattern of patch antenna embedding spiral inductors. W=32 mm, L=32 mm, W_a=3 mm, w_s=s=1 mm, L_a=31 mm, L_s=6.5 mm, L_i=8 mm, h_1=h_2=0.6 mm, d=5 mm, L_1=16.5 mm, L_2=7.5 mm, —: measurement, - - -: simulation.

III. RESULTS

Fig. 4 shows the measured and simulated return loss of the patch antenna embedding spiral inductors. the resonant frequency is 1.905 GHz and the 10-dB bandwidth is 1.6% (1.89-1.92 GHz), which covers the PHS band of 1.895-1.916 GHz. Compared to conventional patch antenna of the same size, the resonant frequencies are reduced by about 60%. The narrow and sharp band enables them to act like filter to reject the noise from adjacent bands.

Fig. 5 shows the radiation patterns, which are very close to those of conventional microstrip antennas. The co-polarization is larger than the cross polarization by 10 dB at $50 \geqq \theta \geqq 0^{\circ}$ and $360^{\circ} \geqq \theta \geqq 270^{\circ}$ on the *E*-plane, and $19^{\circ} \geqq \theta \geqq 0^{\circ}$ and $360 \geqq \theta \geqq 270^{\circ}$ on the *H*-plane. The back radiation is due to the small ground plane that is about five times the area of the patch.

VI. CONCLUSION

In this part, meshed antenna with lumped inductors is proposed, of which the resonant frequency is reduced by about 44% as compared to its counterpart without lumped inductors. A patch antenna embedding round spiral inductors is also proposed, of which the resonant frequency is reduced by 60%. When the round spiral inductors are placed at the center, the resonant frequency can be reduced more significantly. The measured and simulated radiation patterns are close to those of conventional patch antenna at the same frequency.

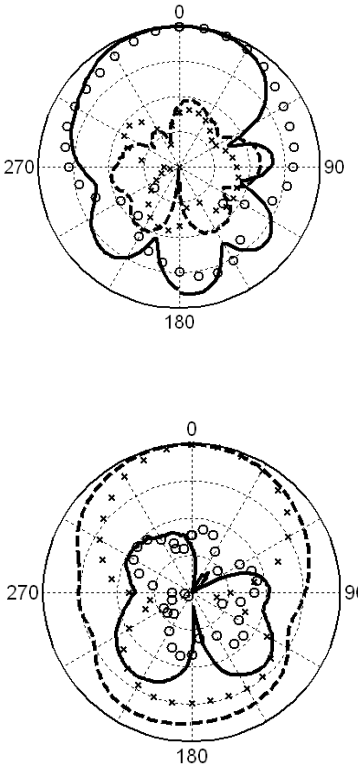

Figure 5 : Radiation pattern of patch antenna embedding spiral inductors. All parameters are the same as in Fig. 4. ---: measured E_θ, - - -: measured E_φ, o: simulated E_θ, ×: simulated E_φ. (a) *E*-plane, (b) *H*-plane.

REFERENCES

[1] C. W. Harrison, "Monopole with inductive loading," *IEEE Trans. Antenna. Propagat.*, vol. 11, no. 7, pp. 394-400, Jul. 1963.

[2] S. T. Best and J. D. Morrow, "Limitation of inductive circuit model representations of meander line antennas," *IEEE AP-S Int. Conf.*, vol. 1, pp. 852-855, June 2003.

[3] N. Behdad and K. Sarabandi, "Bandwidth enhancement and further size reduction of a class of miniaturized slot antennas," *IEEE Trans. Antennas Propagat.*, vol. 52, no. 8, pp. 1928-1935, Aug. 2004.

[4] N. Behdad and K. Sarabandi, "Slot antenna miniaturization using distributed inductive loading," *IEEE AP-S Int. Conf.*, vol. 1, pp. 308-311, June 2003.

[5] R. Azadegan and K. Sarabandi, "A novel approach for miniaturization of slot antennas," *IEEE Trans. Antennas Propagat.*, vol. 51, no. 3, pp. 794-797, Mar. 2004.

[6] R. Azadegan and K. Sarabandi, "Design of miniaturized slot antennas," *IEEE AP-S Int. Conf.*, vol. 4, pp. 565-568, July 2001.

[7] L. G. Young, K. Yonghoon, L. J. Sik, and N. Sangwook, "Size reduction of microstrip-fed slot

antenna by inductive and capacitive loading," *IEEE AP-S Int. Conf*., vol. 1, pp. 312-315, June 2003.

[8] J. L. Volakis, M. W. Nurnberger, and D. S. Filipovic, "A broadband cavity-backed slot spiral antenna," *IEEE Antennas Propagat. Mag*., vol. 43, pp.15-26, Dec. 2001.

[9] M. Manteghi and Y. R. Samii, "Patch antennas using embedded lumped element delay line for size reduction," *IEEE AP-S Int. Conf*., vol. 4, pp. 2-5, June 2002.

[10] S. Schulteis, C. Waldschmidt, W. Sorgel, and W. Wiesbeck, "A small planar inverted F antenna with capacitive and inductive loading," *IEEE AP-S Int. Conf.*, vol. 4, pp. 4148-4151, June 2004.

[11] B. Razavi, *RF Microelectronics*, 1st ed., Prentice Hall, 2003.

Analysis of Range Detection System

Abstract —In this part, a range detection system using frequency-modulated continuous-wave radar is designed at 2.45 GHz. The system consists of low-noise amplifier, local oscillator, mixer and DSP processor. Advanced high-electron-mobility transistors (HEMT) are used in the RF circuit to reduce noise. Specific algorithms are chosen to analyze the echoed signal. Three DSP systems are proposed to reduce the complexity of conventional systems. They are simulated with Matlab, and the results match well with the theoretical prediction.

Index terms — FMCW radar, DSP, range detection.

I. INTRODUCTION

Several types of sensor have been used in range detection, including acoustic, optical , radar, and so on, depending on the environment [1], [2]. The sensors are expected to operate normally in rain, snow, and fog. While infrared and laser waves can penetrate through fog and rain to some degree, their sensitivity severely degrades with contamination on the sensor face [3]. Acoustic sensors are not accurate enough in range resolution. Microwave radars are less vulnerable to bad weather conditions.

The radio waves experience less attenuation through the atmosphere than light, which makes it possible to detect targets far out of visible range [4]. As shown in Fig.1, a radar system transmits an electromagnetic signal which is bounced off the target and captured by the receiver. Some parameters of the signal such as time delay, frequency shift are measured by the receiver to extract information about the target [5].

The frequency band of radars ranges from 3 MHz to 300 GHz, but most radars operate in the microwave frequencies. UHF and VHF radars are used for long-range detection. Search radars and tracking radars often use higher bands for better resolution.

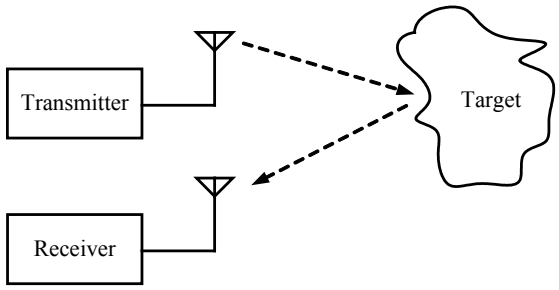

Figure 1: General concept of a radar system.

II. FMCW RADAR

A pulse radar can be used to search, detect, and measure the range of targets. A series of pulses are radiated in certain direction using high-directivity antenna or antenna array. When pulses are reflected by the target, their time delay can be measured to determine the traveling time of the pulse, hence the distance.

However, pulse radar has some disadvantages. For example, wideband antenna is needed to radiate the pulse waveform effectively. Fig.2 shows the principle of linear frequency-modulated continuous-wave (FMCW) radar. The use of frequency modulated signals for range detection was developed in 1920s for ionospheric sounding [6]. The first practical FMCW radar was developed to sense airplane altitude, built by J. O. Bentley [7]. Fig.3 shows the FMCW radar proposed by Bentley. Frequency of the transmitted wave is modulated by a triangular waveform using an electric motor to rotate an adjustable capacitor. The receiver is tuned to match the transmitter for optimum reception. An IF frequency proportional to the altitude of the airplane can be detected at the receiver output. The FMCW radar altimeters were widely used during World War II, and subsequently in civil aircrafts.

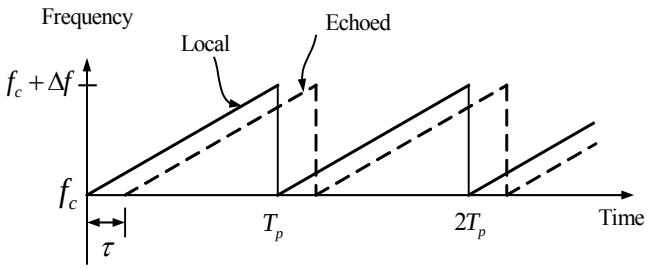

Figure 2: Principle of range detection system using FMCW.

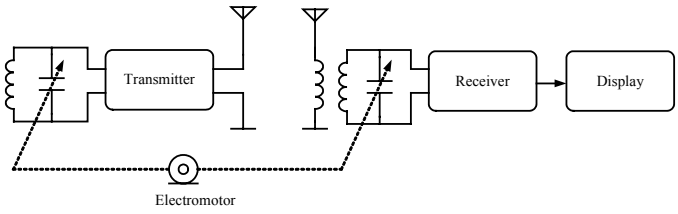

Figure 3: Schematic of radio altimeter by Bentley.

III. PROPOSED SYSTEM

In FMCW radar systems, range resolution depends on the sweep bandwidth, the receiver frequency resolution, and the linearity of frequency sweep. Nonlinearity of frequency sweep is often the limiting factor in FMCW radar range resolution. The varactor in VCO is a nonlinear device, hence, the output frequency of the VCO is not a linear function of the input voltage. Conventional FMCW systems use supplemental VCO linearization circuit to calibriate the output frequency of VCO, which increases circuit complexity and system cost. In this work, the VCO is controlled by the DSP using algorithms to achieve linear frequency sweep.

Fig.4 shows an improved FMCW system which uses DSP to generate a periodical waveform to drive the voltage-controlled oscillator. The waveform is well tuned to linearize the output frequency of the VCO. Feedback circuit can be used to facilitate the fine-tune. The linearized RF FMCW signal is sent to a power divider to feed the transmitting antenna and the mixer, respectively. The reflected FMCW signal is received by the antenna, fed into the receiver through the circulator, amplified to an appropiate level to be mixed with the local signal. An auto-gain-control (AGC) amplifier can be incorporated to extend the detection range. The mixer output is low-pass filtered to eliminate the spurious high-frequency components. Another IF amplifier with auto-gain control is used to raise the signal level for better analog-to-digital (ADC) conversion. Proper algorithms are developed to determine the frequency difference.

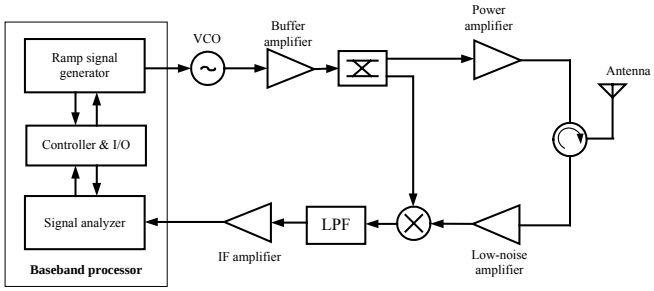

Figure 4: FMCW system with DSP-generated sweep waveform.

Utilizing DSP and high-speed DAC, FMCW signal can be generated at lower frequency band digitally and up-converted to the RF band to be transmitted. Fig.5 shows the architecture of the proposed FMCW system. The voltage-controlled oscillator in Fig.4 is replaced with a local oscillator and an up-conversion mixer. There are several advantages with this modification. First, the operation of a voltage-controlled oscillator usually requires voltage swing of 10 V or higher, while the fixed-frequency local oscillator is easier for design and implementation. Secondly, supplemental linearization and feedback circuits are not required in the proposed system, which significantly decreases the circuit complexity and system cost.

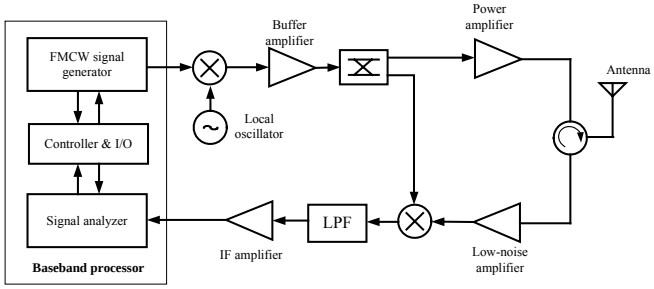

Figure 5: FMCW system with digital IF waveform.

In short-rangen, detection of frequency difference becomes impossible due to the phase noise if the transmitted and recieved RF freqeuencies are too close. In order to overcome this problem, a two-stage heterodyne receiver as shown in Fig.6 is used instead of the homodyne receiver. The DSP generates an FMCW waveform with frequency swing on the order of 10 MHz, up-converted to 2.45 GHz band to be transmitted. The received signal is mixed with the same LO signal. The IF signal at the mixer output contains the delayed version of the FMCW waveform and its harmonic. After low-pass

filtering, the IF signal is sampled and sent to the DSP, multiplied with the FMCW waveform. The range can be determined by applying the spectral analysis algorithm.

The enhanced accuracy is brought by the DSP which multiplies signals with less distortion than achieveable by analog circuits. Such enhanced accuracy will enable the system to detect targets at closer range. Frequencies measured by the system can be increased to further improve accuracy.

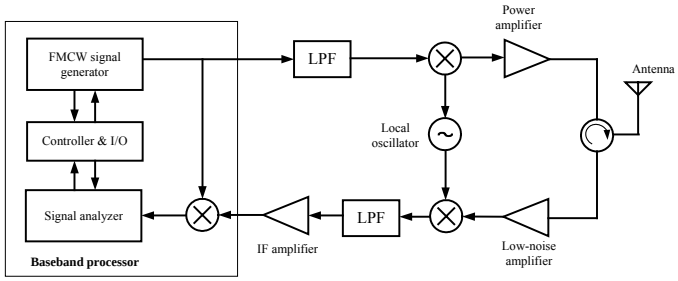

Figure 6: FMCW system with digital IF and digital mixing.

IV. SIMULATION RESULTS

The proposed FMCW systems are simulated using Matlab. The detection range is set to 6 m for experiment in an anechoic chamber. The center frequency and frequency swing of FMCW waveform is 2.45 GHz and 50 MHz, respectively.

The radar range equation is used to estimate the received power, which incorporates antenna parameters, target characteristics, and distance. Narrowband additive white noise at room temperature is used to model the noise of the system. Frequency response is assumed to be constant with power divider, power amplifier, circulator and antenna in the frequency band of interest. Only the amplitude attenuation and time delay are considered in the channel model. Narrowband white-Gaussian noise is assumed in the channel. Multipath effect of the FMCW wave is not considered if the system is to be tested in an anechoic chamber. The leakage power from the transmitter to the receiver through circulator is ignored. In practice, the leakage may be a critical interference.

The architecture of FMCW system using DSP shown in Fig.4 is simulated. A sawtooth ramp waveform is simulated to control the ideal voltage-controlled oscillator with phase noise of -100 dBc/Hz at 100 kHz offset. The radiated spectrum of the FMCW wave is shown in Fig.7. Note that the spurious signals and distortion incurred by the nonlinearity of the RF components are neglected.

Fig.8 shows the signal spectrum at the output of the local mixer. Two salient components are observed in the spectrum. One is a desired IF component near dc, the other is the second harmonic generated by the mixer. The high-frequency spurious signal can be rejected by using a low-pass filter with the cutoff frequency of 100 MHz.

The filtered signal is sent to the analog-to-digital (A/D) converter. The IF frequency can be accurately determined by applying the Hamming window and Welch periodogram in the spectral analysis algorithm. The signal is divided into four data segments, each with 8,000 samples. The overlap between adjacent segments is one-fourth a period, namely, 2,000 samples. As shown in Fig.8, the IF signals have peaks at 20 kHz, 40 kHz, 60 kHz, and 100 kHz, respectively, match well with the theoretical prediction. The IF frequency increases in proportion to the distance to the target.

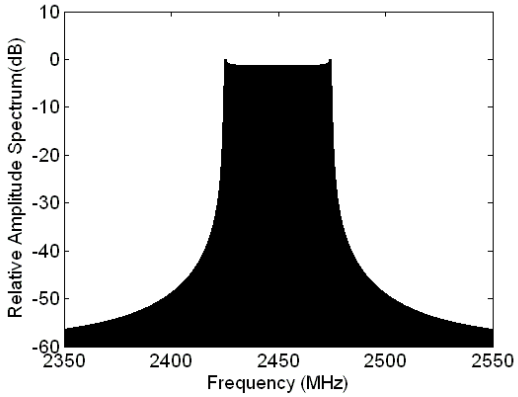

Figure 7: Radiated spectrum using the architecture in Fig.4.

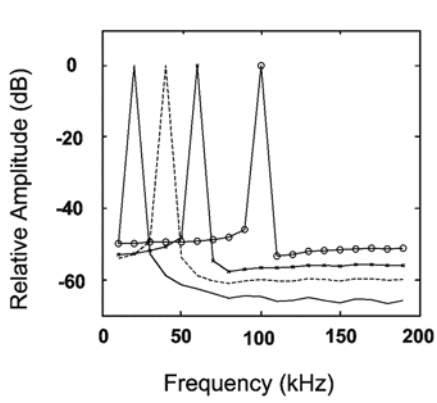

Figure 8: IF spectrum with the architecture in Fig.4, determined by Hamming window and Welch periodogram, -:target at 6 m, --:target at 12 m, -x-:target at 18 m, -o-:target at 30 m.

Next, consider the system shown in Fig.5 in which the FMCW signal is generated from the baseband signal generator. The baseband FMCW wave is mixed with a constant-frequency LO signal at 2.45 GHz to generate the RF FMCW wave. Gaussian noise is added to a pure sinusoidal wave to simulate the LO signal with phase noise -100 dBc/Hz at 100 kHz offset.

Hamming window and Welch periodogram are applied in the spectral analysis algorithm. The samples are divided into four data segments, each with 8,000 samples. The overlap between adjacent segments is one-fourth a period, namely, 2,000 samples. Fig. 9 shows that the IF signals have peaks at about the same frequencies as in Fig.8.

V. CONCLUSIONS

In this work, a frequency-modulated continuous-wave (FMCW) radar is used for range detection. The FMCW radar has the advantage of low power and high resolution.

Three different systems have been proposed to improve conventional FMCW systems. Advanced high-electron-mobility transistor (HEMT) is used to reduce noise. The phase noise of the local oscillator is -100 dBc/Hz at 100 kHz offset. This ensures the sensitivity of the range detection system.

Specified periodogram algorithm with pseudo ensemble averaging technique is used to analyze the echoed IF signal to determine the target range. The data segments are overlapped to improve the stability of the spectrum. The systems are simulated using Matlab to verify the performance. The results match well with theoretical prediction.

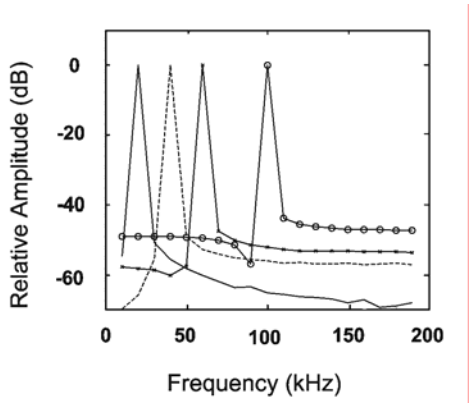

Figure 9: IF spectrum with the architecture in Fig.5, estimated by Hamming window and Welch periodogram, -:target at 6 m, --:target at 12 m, -x-:target at 18 m, -o-:target at 30 m.

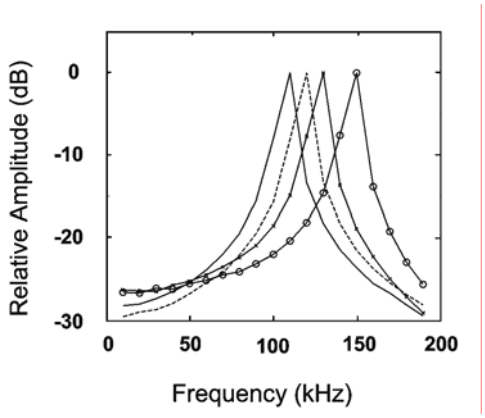

Figure10: IF spectrum with the architecture in Fig.5, estimated by Hamming window and Welch periodogram, -:target at 6 m, --:target at 12 m, -x-:target at 18 m, -o-:target at 30 m.

REFERENCES

[1] C. Metz, J. Grubert, J. Heyen, A. F. Jacob, S. Janot, E. Lissel, G. Oberschmidt, and L. C. Stange, "Fully integrated automotive radar sensor with versatile resolution," *IEEE Trans. Microwave Theory Tech.*", vol. 49, no. 12, pp. 2560-2566, Dec. 2001.

[2] E. Moldovan, S. O. Tatu, T. Gaman, K. Wu, and R. G. Bosisio, "A new 94-GHz six-port collision-avoidance radar sensor," *IEEE Trans. Microwave Theory Tech.* , vol. 52, no. 3, pp. 751-759, Mar. 2004.

[3] L. V. Blake, *Radar Range Performance Analysis*, Artech House, 1986.

[4] D. K. Barton, *Modern Radar System Analysis*, Artech House, 1998.

[5] N. S. Tzannes, *Communication and Radar Systems*, Prentice Hall, 1985.

[6] I. V. Komarov and S. M. Smolskiy, *Fundamentals of Short-Range FM Radar*, Artech House, 2003.

[7] J. O. Bentley, '*Airplane Altitude Indicating System*,' U. S. Patent no. 2,011,392, Aug. 13 1935, application Aug. 10 1928.